

The Near Infrared Spectrum of Miranda

Evidence of Crystalline Water Ice

James M. Bauer¹

Institute for Astronomy, University of Hawaii, 2680 Woodlawn Drive, Honolulu, Hawaii 96822
E-mail: bauer@ifa.hawaii.edu

Ted L. Roush

Space Science Division, Planetary Systems Branch, Mail Stop 245-3, NASA Ames Research Center, Moffet Field, California 94035-1000

Thomas R. Geballe¹

Gemini 8-Meter Telescope Project, 670N. A'ohoku Place, Hilo, Hawaii 96720

and

Karen J. Meech, Tobias C. Owen,¹ William D. Vacca,² John T. Rayner,² and Kevin T. C. Jim

Institute for Astronomy, University of Hawaii, 2680 Woodlawn Drive, Honolulu, Hawaii 96822

Received March 13, 2001; revised February 19, 2002

A spectrum from 1.2 to 2.5 μm of Uranus' small satellite Miranda obtained in June 1999 reveals strong water-ice signatures. It confirms the existence of a 2.0- μm water feature previously detected on Miranda and shows a strong second broad 1.5- μm water-ice absorption feature. The spectra also reveal a weak absorption band at 1.65 μm that is indicative of crystalline water ice. Reflectance models which combine the new spectra with new photometry indicate that the spectra are characteristic of a mostly water-ice surface, with a large fraction of carbonaceous or silicate contaminants, and the possible presence of ammonia hydrate, as implied by an apparent weak feature near 2.2 μm . The possible presence of other volatiles is also investigated. © 2002 Elsevier Science (USA)

Key Words: Uranian satellite; outer Solar System; water.

1. INTRODUCTION

Recent spectral studies of the Centaurs Chariklo and Pholus (R. H. Brown *et al.* 1998, Brown and Koresko 1998, Cruikshank *et al.* 1998a), and of the outer-planet satellites such as Nereid (R. H. Brown *et al.* 1999, M. E. Brown *et al.* 1998) and Phoebe (Owen *et al.* 1999), consistently yield evidence of water ice on the surfaces of these small bodies, particularly from detection of

the 2.0- μm absorption band. However, the abundance of water ice on their surfaces as indicated by the absorption band depths varies greatly from object to object. Likewise the presence or absence of other volatile materials is also highly variable from object to object.

There are several different models for the formation of the uranian and outer-planet satellite systems, and each theory predicts a different subnebular chemistry which could account for the variety in the observed water-ice abundances. Pollack *et al.* (1991) present several scenarios for the uranian satellites. In the accretion disk model, the satellites form from the outer solar nebula gas and solids which become gravitationally trapped by Uranus. Here, CO is the principal C-bearing species, and the temperatures are too low to convert CO to methane and water. In the spin-out disk model, the satellite forming disks are remnants of the outer-planet envelopes. Determining the probable starting composition for the satellites depends on understanding the convective mixing in the envelope and the protoplanet luminosity. The temperatures and pressures in this scenario were probably high enough for C and N to be fully reduced, with CH₄ and NH₃ as the dominant C- and N-bearing species. In a third scenario, the satellite-forming disk could have been generated during the impact that gave Uranus its high obliquity. In this model, shock heating would have converted much of the CH₄ to CO in the envelope of the planet and would have depleted the disk in water, resulting in a higher rock-to-water ratio in the satellites. Finally, in the co-accretion model, the satellite origin is similar to that

¹ Visiting Astronomer, United Kingdom Infrared Telescope, Joint Astronomy Center, Hilo, Hawaii.

² NASA Infrared Telescope Facility (IRTF), Institute for Astronomy, Honolulu, Hawaii.

of the accretion model, except that there is a larger fraction of planetesimals, hence organics, incorporated into the satellites. From these models, one may expect to see a trend in composition as one progresses from the inner satellites, formed *in situ*, to outer, likely captured, satellites and Centaur bodies which were formed in the outer protostellar nebula, away from protoplanetary formation. Understanding the satellite composition can allow us to constrain scenarios of formation.

Miranda is a particularly interesting case study of such theories. The innermost of Uranus' major satellites and the smallest, Miranda was first discovered in 1948 by Gerard Kuiper (see Kuiper 1949). The satellite has a radius of 235.8 ± 0.7 km, and mass estimates from Voyager 2 Doppler tracking data (Jacobson *et al.* 1992) indicate a density close to that of water ice, $\rho = 1.15 \pm 0.15$ g cm⁻³, thus making Miranda the least dense of the major uranian satellites. The density suggests a rock mass fraction between 0.2 and 0.4. Voyager images revealed a bizarre surface with extensive old heavily cratered terrain cut by tectonic features and features of probable volcanic origin, suggesting that it has been thermally altered since formation. Unusual geologic regions called coronae exist, relatively uncratered compact areas 200–300 km across surrounded on all sides by a network of extensional rifts. The rifting is extant over the portion of the surface imaged (e.g., Helfenstein *et al.* 1988). The coronae are probably tectonic features which have been modified volcanically.

The first near-IR observation of Miranda was a 16-band spectrum ranging from 1.6 to 2.4 μm , which revealed a 2.0- μm feature attributed to water ice (R. H. Brown and Clark 1984). In the Voyager images, the heavily cratered regions external to the slightly reddish coronae were found to be relatively blue (Buratti *et al.* 1990, Buratti and Mosher 1991). Subsequent ground-based observations (Buratti *et al.* 1992) revealed a strong opposition surge in brightness at optical wavelengths indicative of a "fluffy" porous surface. The JHH'K photometry of Baines *et al.* (1998) showed that the opposition effect likely extends into the infrared. A fluffy, multiply cratered surface may imply a history of bombardments by small bodies. The observed opposition effect may alternatively be caused by a thin covering of volatile frost. The more recent seven-color optical photometry of the uranian satellite system by HST (Karkoschka 1997) confirmed the slightly blue color of Miranda's full disk, in marked contrast to the red colors of other uranian satellites in the system and most Centaurs (Davies *et al.* 1998).

The average normal albedo of the surface from Voyager is $p_v \sim 0.33$ (representative of the older, heavily cratered terrain) and varies from 0.30 to 0.37 (Buratti and Mosher 1991). Voyager's observations showed that the surface was spectrally flat between 0.4 and 0.6 μm (Veverka *et al.* 1991). It has been speculated that the composition of the dark material may represent radiation-darkened (polymerized) CH₄ (Veverka *et al.* 1991).

Geologic structures and cratering records help us infer the thermal histories of the uranian satellites. Models of expansion both prior to melting and volcanism and after melting suggest

that the satellites may have expanded by as much as 2%. The associated temperature rise would have been $\Delta T \sim 100$ K for both pre- and postmelting (Croft and Soderblom 1991). Miranda's volatiles cannot consist of pure water, because the modeled ΔT would have required complete melting of the ices, erasing any premelt surface features (which are preserved in the old, cratered terrain). Likewise, refreezing of pure water ice would have resulted in an expansion twice as large as suggested. Therefore, the presence of a more volatile material, such as ammonia hydrate (NH₃ · H₂O), is suggested.

The presence of material more volatile than water is also inferred because water ice has a high thermal conductivity and high melting point, and it is difficult to trap enough heat in Miranda to explain the tectonic activity. Radioactive heating of water ice alone would not have been sufficient, resulting in a ΔT of only 10–20 K (Tittlemore and Wisdom 1990). Marcialis and Greenberg (1987) and Tittlemore and Wisdom (1990) proposed that Miranda's passage through orbital resonances, specifically with Umbriel, may have heated its core to 200 K from 80 K. However, this temperature would not be high enough to melt a pure water-ice body the size of Miranda, without a sufficient amount of more volatile materials (such as ammonia hydrate). If volatiles such as nitrogen, methane, or carbon monoxide were present in the ices in addition to ammonia, the cryomagma should have been loaded with gases, and there would be evidence for explosive volcanism, which is not seen on Miranda. On Miranda, while the estimated volume of cryomagmas is relatively small, the possible minor volatiles might be volumetrically important surface deposits, and we might expect to find evidence for ammonia or other volatile absorption in the spectra. One may expect to find C–H-bearing species, such as methanol, if Miranda formed in a CH₄-rich environment. One would not expect to find pure methane, since it would have evaporated from the surface in less than a few million years (see, for example, M. E. Brown 2000).

The error bars on the earlier spectroscopic data were too large to draw any inferences about the presence of more volatile materials (e.g., CH₄ or NH₃) on the surface of Miranda, and in fact the data allow up to a few percent of the more volatile materials to be mixed with the water ice. Because of the importance of composition in understanding the thermal history, evolution, and formation of the uranian satellites, we have obtained near-IR observations of Miranda to search for trace constituents in the spectra and study the presence of water ice in more detail.

2. OBSERVATIONS AND DATA REDUCTION

2.1. Spectra

We observed Miranda using the 3.8-m United Kingdom infrared telescope (UKIRT) on Mauna Kea. The observations took place during the second halves of the nights of UT 1999 June 7 and 10. We used the facility spectrometer, CGS4, a 1- to 5- μm multipurpose two-dimensional grating spectrometer containing a 256 × 256 InSb array detector. Both nights were clear, and

TABLE I
Observing Geometry and Instrumental Configuration

Parameter	June 7, 1999	June 10, 1999
Separation from Uranus	9''	9''
Position angle (N → E) ^a	155°–168°	181°–195°
Phase angle	2.52°	2.47°
Spectral range (resolving power)	1.83–2.47, 1.43–2.07 μm ($\lambda \times 200$), ($\lambda \times 200$)	1.01–1.33, 1.43–2.07 μm ($\lambda \times 400$), ($\lambda \times 200$)
Slit dimensions	1.2 \times 90''	1.2 \times 90''
Grating ruling	40 lines/mm	40 lines/mm
Slit pos. angle	90°	90°

^a PA of Miranda relative to Uranus.

seeing was less than 1''. The observing geometry is shown in Table I. Miranda's visual magnitude was listed by the JPL's Horizon ephemeris as $m_v = 16.5$.

We aligned the slit within 20° (PA \sim 90°) of the tangent to Miranda's motion about Uranus on the sky plane. This orientation allowed the array to sample spectra of background-scattered light from Uranus parallel to and on either side of Miranda's spectral signal rows. The instrumental configuration has been summarized in Table I.

Three spectral segments (1.01–1.33, 1.44–2.08, and 1.84–2.48 μm ; hereafter the 1.2- 1.8- and 2.2- μm bands, respectively) were observed. For each band a series of exposures were obtained with Miranda centered in two different rows separated by 7''. Individual exposure times were 40 and 60 s. The total exposure times in these bands were 1920, 2400, and 2560 s, respectively. The star HD 198802 (G1V) was used as a spectroscopic standard (Colina *et al.* 1996). It was observed immediately before each series of Miranda exposures and at airmass values within a few hundredths of that of the Miranda observations. Flat field exposures and arc lamp exposures (for wavelength calibration) were obtained after each change in instrumental set-up.

The CGS4 online reduction software was used to flatten, remove bad pixels from, and combine the individual frames. For each spectral band a final coadded frame was produced online by summing pairs of subtracted frames; each coadd contains positive and negative spectra of Miranda (or the calibration star) separated by 12 rows of the array, along with residual sky background. Subsequent extraction of the positive and negative spectra and their subtraction to form final spectra removes the residual sky emission, apart from that due to the nonuniformly distributed scattered light from Uranus (see below). The combined spectra were wavelength-calibrated using the arc lamp spectra. Nontelluric absorption lines in the standard star were removed. The Miranda spectra were then flux-calibrated by dividing them by the standard star's spectra and multiplying them by a black body curve of the same temperature as the standard star's stellar atmosphere (Allen 1973).

Figure 1a shows the overall shape and spectral energy distribution across all three spectral bands, which seem to grossly align. However, it is clear from the overlap between the 2.2- and

1.8- μm spectral bands that slight offsets remain. The slight offset may be caused by changes in the seeing and guiding accuracy, such that the same fraction of the flux from Miranda and the flux calibration star may not have fallen within the narrow slit, or by differences in brightness or temperature from the canonical G1V spectral type of our solar analog standard, HD198802. However, the two 1.8- μm flux spectra from the separate nights of June 7 and June 10 do closely overlap. The mean difference between the signals was 5% and they needed no rescaling relative to each other before their signals were averaged. Figure 1a also shows the major telluric, solar, and strong Uranus background feature regions which may have introduced errors at those wavelengths in the extracted spectrum. We choose not to artificially rescale the 2.2- μm spectra upward in our flux values shown in Fig. 1a

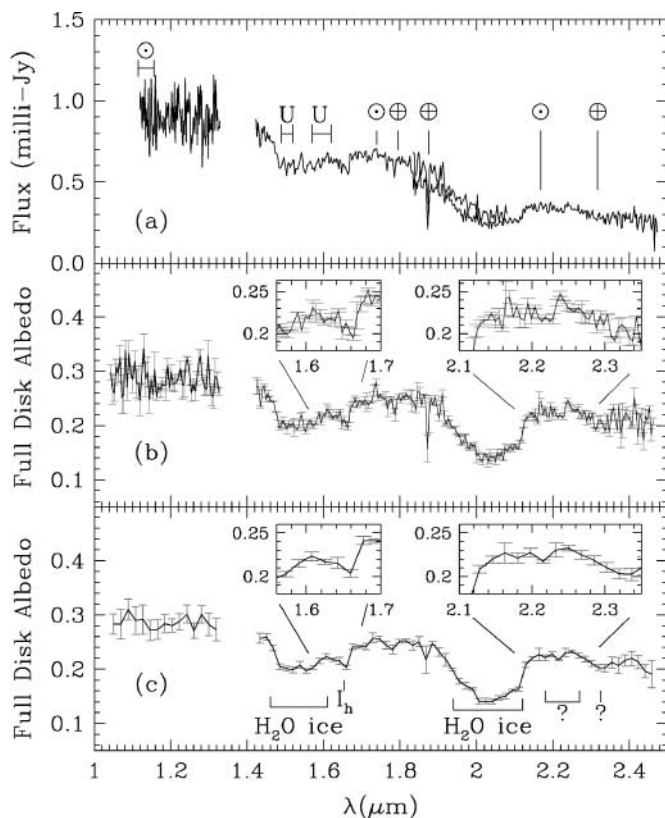


FIG. 1. The CGS4 spectral data. (a) The CGS4 data flux values from 1.1 to 2.5 μm , from June 7 and 10, 1999. The data have not been rebinned. There are no overlap regions between the 1.2- and 1.8- μm bands, as there are for the 1.8- and 2.2- μm bands. The wavelengths where some major telluric (\oplus), solar (\odot), and strong Uranus background (U) features were located in the unreduced data are indicated here as well. (b) The relative reflectance of Miranda across the three bands (averaged for June 7 and 10), from 1.1 to 2.5 μm , with statistical errors shown. The errors for each resolution element were taken from the dispersion in the values averaged to the rebinned value. The data were binned to the instrument's resolving power ($\Delta\lambda \sim 0.005 \mu\text{m}$). (c) Data binned to a resolving power of about a quarter of the instrument's resolving power ($\Delta\lambda \sim 0.02 \mu\text{m}$). Major features discussed in the text are indicated in both (b) and (c). At the lower resolution, features near 1.65 (hexagonal water ice, I_h), 2.2 and 2.3 μm are still present with SN $> 2\sigma$. The insets in both figures show the expanded spectrum near the 1.65- and 2.2- μm features.

since the offset is so slight that it is of little consequence to our conclusions. Note, however, that to show spectral features better in Figs. 1b and 1c, we do rescale the flux by a factor of 1.2 before calculating our relative reflectance values.

Scattered light from Uranus and its rings contributed significant background contamination, particularly in the 1.2- and 1.8- μm bands. This was removed by using a fifth-order background function fit to three regions perpendicular to the dispersion direction. This includes an extra region in between the positive and negative signals, as opposed to using just the usual two sample regions on either side of the object positive and negative spectrum signal. The worst contamination occurred in the 1.2- μm band, where the CH_4 absorption from Uranus is weakest. We were unable to properly extract Miranda's spectra shortward of 1.1 μm owing to Uranus' background-scattered light. Within the 1.8- μm spectral band, Uranus' background becomes strongest near 1.5–1.64 μm (see Fig. 1a). Hence near 1.50 and 1.61 μm we encountered problems fitting the background, the first night undersubtracting and the second night oversubtracting. The spectral flux values were divided by a solar spectrum (Colina *et al.* 1996) and multiplied by a distance scaling factor (e.g., Roush *et al.* 1996) to arrive at the relative reflectance values. The relative reflectance values are in units of full disk albedo (ρ_λ) calculated as

$$\rho_\lambda = \frac{r^2 d^2}{R^2} \frac{\mathcal{F}_0}{[\mathcal{F}_\odot \cdot (1\text{AU})^2]}, \quad (1)$$

where \mathcal{F}_0 and \mathcal{F}_\odot are the satellite's measured flux and the solar flux at Earth, respectively, r (AU) and d (AU) are the heliocentric and geocentric distances, and R (AU) is the object radius.

The last two panels, Figs. 1b and 1c, show the statistical errors calculated by taking the dispersion in the data points as they are rebinned to wavelength intervals of (Fig. 1b) one and (Fig. 1c) four resolution elements. No spectral signature of Uranus or its rings appears to remain in the spectra. The 1.2- μm band spectrum has no overlapping values with the 1.8- μm data and has only a single set of exposures taken on the second of the two nights. Hence, the relative offset of the 1.2- μm albedo values to those of the 1.8- and 2.2- μm data is suspect, by order ± 0.02 , which is the range in values we encountered when using different extraction and background fitting techniques. We calculated broadband near-IR photometry values from our spectra and later obtained near-IR photometric observations to verify the alignment of our 1.2- μm spectra with our overlapping 1.8- and 2.2- μm spectra (Section 2.2).

2.2. Photometry

To obtain our J, H, H' ($\lambda_{\text{central}} = 1.72 \mu\text{m}$), and K band reflectance values, we multiplied the UKIRT data with the IRTF filter transmission data for the corresponding filters. For J values, we used the J_{mk} filter transmission data in place of the older filter transmission values, since this newer filter was a better match to our 1.2- μm band data set. The errors include the statistical er-

TABLE II
Full Disk Albedos

λ (μm)	Albedo	σ	λ_{FWHM}
UKIRT CGS4 (June 1999)			
1.247	0.260	0.018	0.16
1.618	0.202	0.010	0.28
1.725	0.225	0.010	0.10
2.203	0.181	0.010	0.40
IRTF SpeX (May 2000)			
1.62	0.243	0.016	0.28
2.20	0.206	0.020	0.40
UH QUIRC (May 2000)			
1.27	0.281	0.028	0.16
1.62	0.224	0.025	0.28
2.20	0.184	0.025	0.40

rors of the individual measurements in each band as reported in Table II. For the J band, the reported error also includes the 0.02 uncertainty from our estimate of the offset of the 1.2- μm spectral band from the 1.8- and 2.2- μm data described in the previous section. The systematic errors owing to not having Miranda and the calibration star equally well centered in the slit or caused by changes in the focus or seeing could be larger than the statistical errors. However, as mentioned in Section 2.1, the difference between the 1.8- μm spectra taken on separate nights was a few percent, much less than the reported statistical errors for the H and H' band photometry derived from that spectral segment.

Figure 2a shows our full disk albedo values (p) of the broadband data derived from our spectral observations at phase angle 2.5° in comparison to values reported in Karkoschka (1997), Kesten *et al.* (1998), and Baines *et al.* (1998) from 0.3 to 2.5 μm at phase angle 1° . The open circles, squares, and triangles show the data obtained at 1.0° , and the filled circles show our UKIRT data. Because the observations from the literature shown in Fig. 2a were obtained at different phase angles resulting in different albedos, we compare the colors of our observations to those previously reported. As the J band spectral segment does not overlap the 1.8- μm band spectrum, there is some uncertainty in the colors including J. The H'-K color derived from the broadband spectral reflectance values of the UKIRT spectra ($p_{H'-K} = 0.04 \pm 0.01$) agree within the formal errors with values reported by Baines *et al.* (1998) ($p_{H'-K} = 0.05 \pm 0.01$). However, the data of Baines *et al.* (1998) yielded J-H' values ($p_{J-H'} = -0.08 \pm 0.02$) significantly different from ours ($p_{J-H'} = 0.04 \pm 0.02$, Fig. 2a). This motivated us to confirm our flux calibration with broadband photometry measurements. We acquired JHK photometry measurements using the QUIRC instrument on the UH 2.2-m telescope and measured the H and K band magnitudes in the IRTF SpeX first light images taken on May 18, 2000. Both QUIRC and SpeX use Mauna Kea (mk) NIR filter sets. QUIRC is the University of Hawaii's 1024 \times 1024 HgCdTe NIR camera. At the $f/10$ focus configuration that we used on the night of May 22, 2000, the camera's field

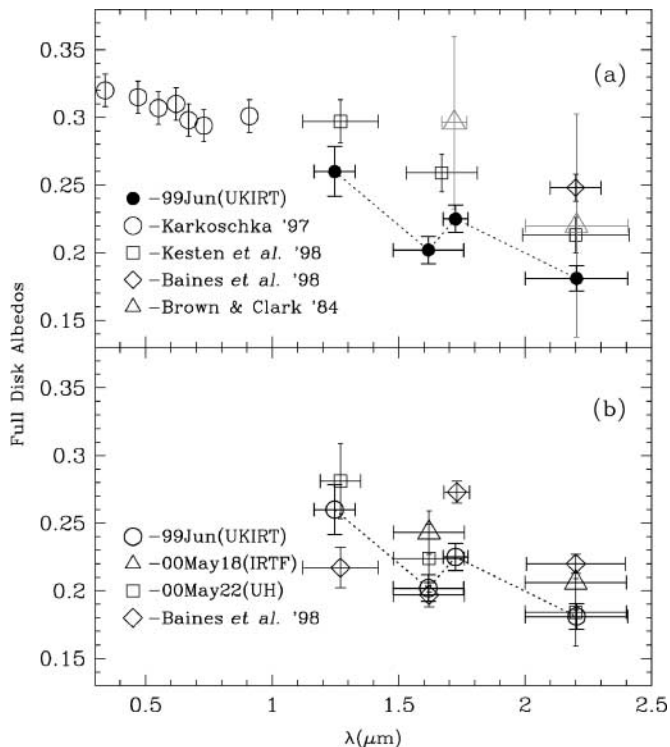


FIG. 2. (a) Optical and near-IR full disk albedos derived from recent broadband photometry data, from 0.3 to 2.5 μm at 1° phase angle from Karkoschka (1997) (open circles), Kesten *et al.* (1998) (open squares), and Baines *et al.* (1998) (open diamonds). The filled circles are the photometry values derived from our spectral data, at 2.4° phase angle shown here for comparison. The Kesten *et al.* data were converted from reported magnitudes into full disk albedo values. The R. H. Brown and Clark (1984) data are shown as open triangles, with gray error bars. Horizontal “error bars” represent the width of the bandpass. (b) Optical and near-IR full disk albedos derived from recent broadband photometry data at 2.4° – 2.9° phase angle including the data reported here and from Baines *et al.* (1998, open diamonds). The UKIRT values are shown as open circles, the UH QUIRC values as open squares, and the IRTF SpeX values as open triangles.

of view is approximately 193×193 arcsec. The imaging array on the IRTF’s SpeX instrument (Rayner *et al.* 1998) is a 512×512 InSb array with a 1 square arcmin field of view. During both observing runs, the telescope was jittered in such a way that Miranda was never on a part of the array previously occupied by Uranus. Sky background was subtracted using median filtered sets of images from immediately before and after each exposure. Both sets of images were reduced in a similar standard fashion, correcting for airmass extinction and zero point offsets using NIR photometric standard stars. We took care to sample the background at identical distances from Uranus. The proximity of a background star prevented us from making use of the SpeX J band image. Because of the combined scattered light gradients from both the star and Uranus, we were unable to make the appropriate corrections for a smaller aperture size which would contain only Miranda’s signal and were unable to properly characterize the background signal in the photometry aperture. The albedo and colors computed from these data, in-

cluding the unscaled UKIRT values derived from the spectra in Table II, are shown in Fig. 2b in comparison with data from Baines *et al.* (1998) taken at nearly the same phase angles (2.4° – 2.8°). Miranda’s projected angular diameter in all instances was less than $0''.04$. The seeing for the QUIRC data was $0''.6$ and for the SpeX data was $0''.7$. In the case of the UKIRT spectroscopy, the $1''.2$ aperture encompassed the entire disk. This was also the case for the photometry with the QUIRC and SpeX data, where we used synthetic apertures of $3''$ or greater. This synthetic aperture size was greater than 3.5 times the FWHM of Miranda in the imaging frames, so that more than 99% of the light fell within the aperture. For the UKIRT data, as mentioned before, a flux calibration star was observed with identical aperture size to properly scale the observed brightness values.

The Kesten *et al.* (1998) values show a significant blue color gradient for the JHK band data (J–H: 0.038 ± 0.021 , H–K: 0.046 ± 0.019 , J–K: 0.084 ± 0.021), as do recently reported observations of Trilling and Brown (2000), taken at a phase angle of 1.5° (J–H: 0.077 ± 0.022 , H–K: 0.020 ± 0.028 , J–K: 0.097 ± 0.027). The Baines *et al.* (1998) data show weak gradients of varying sign for J–H (0.020 ± 0.017), H–K (-0.023 ± 0.011), and J–K (-0.003 ± 0.016). The QUIRC (J–K: 0.057 ± 0.038 , H–K: 0.040 ± 0.035 , J–K: 0.097 ± 0.038), SpeX (H–K: 0.037 ± 0.026), and UKIRT (J–K: 0.06 ± 0.022 , H–K: 0.02 ± 0.014 , J–K: 0.08 ± 0.022) show consistently blue color gradients which agree with each other and the Kesten *et al.* (1998) values within the reported errors and disagree, except for the J–H color value, with the Baines *et al.* (1998) data. This discrepancy may be caused by several factors, including the sampling of unique surface regions (see Section 4.1) by the Baines *et al.* (1998) observations, or the mismatch of filter bandpasses between the data sets from the different observers. It should also be noted that the individual SpeX points are significantly brighter than the H and K albedo values derived from the UKIRT spectra, which may also be attributable to observations of Miranda at times when the subobserver points were well separated and on characteristically different portions of that satellite’s surface (Fig. 5).

3. ANALYSIS

3.1. Identification of Spectral Features

The spectrum of Miranda exhibits several characteristics that we recognize and consider in our modeling effort (Figs. 1b and 1c). The broad minima located near 1.5 and 2.0 μm are present in both amorphous and crystalline water-ice spectra (e.g., Cruikshank *et al.* 1998b, Schmitt *et al.* 1998, Grundy and Schmitt 1998). Additionally, the weaker feature near 1.65 μm coincides with a feature found only in the spectrum of the crystalline form of water ice at low temperatures (Schmitt *et al.* 1998, Grundy and Schmitt 1998). An even weaker feature near 2.22 μm coincides with features observed in ammonia ice at 2.24 μm and solid ammonia hydrate at 2.21 μm (e.g., Schmitt *et al.* 1998, R. H. Brown *et al.* 1988). To check the persistence of these features, we rebinned the spectrum to about one-quarter the instrumental resolving power (Fig. 1c). The 1.65- μm

crystalline ice and 2.22- μm features remain apparent, with signal-to-noise (SN) values of 2.9 and 4.3 respectively when the feature minima are compared with proximal peaks or edges. We show data with the degraded spectral resolution here only for comparison and use the spectrum at the full instrumental resolving power (Fig. 1b) for our modeling fits.

In the higher resolution spectrum (Fig. 1b) the possibility of a weak feature near 2.33 μm may indicate the presence of a CH-bearing species or perhaps a hydroxylated silicate. This feature remains apparent in the lower resolution binning of the data with a SN near 2.8. A couple of sharp, but weak features at 2.01 and 2.07 μm , which have SN values in the higher resolution data of 1.5 and 1.9, respectively, might be attributable to CO₂ ice, but an expected CO₂ feature at 1.965 μm appears weak or absent. Furthermore, while the 2.01- μm feature in both 1.8- μm spectra from separate nights may be due to the actual presence of CO₂ ice, the absence of this CO₂ feature in the 2.2- μm spectra argues against this, and so we find our spectra are inconclusive in the detection of CO₂ ice. These features are narrow and do not persist in the low-resolution sampling of the spectrum. The overall level of Miranda's albedo suggests a darkening agent that does not exhibit any color trends at the shortest wavelengths.

3.2. Spectral Modeling

To provide insight into the nature of the surface material(s) on Miranda we have produced model spectral albedos for different candidate materials and their associated grain size(s) to compare with the new data. The model used is that originally developed by Hapke (e.g., Hapke 1993) to describe the measured albedo. The details describing the formulation used in our effort are provided by Roush *et al.* (1990), Roush (1994), and Cruikshank *et al.* (1998a). The limited phase angle coverage of near-infrared wavelengths precludes us from independently determining some of the parameters of the models. Here we rely upon values of these parameters derived from Voyager observations by Helfenstein *et al.* (1988); specifically the parameters, as defined in Roush (1994), have the values $b = 0.93$, $h = 0.018$, and $S_0 = 0.77 \times$ (Fresnel reflectance). This approach also requires that the real and imaginary indices of refraction of candidate materials be specified. The availability of appropriate optical constants is limited, constraining our range of model computations. Nonetheless, different wavelength regions of the Miranda spectrum allow us to investigate a range of plausible candidates. The reflectance model is coupled to a downhill simplex algorithm (Press *et al.* 1992) that in a single run autonomously investigates a range of parameter values to define the best fit to the data in a least squares sense. When appropriate, the same components, but having different initial estimates of relative abundance and grain size, are used to confirm that the simplex has reached the same result. We have eliminated two data points near 1.8 μm from the original spectral observations due to their high variance and association with strong telluric features.

In our modeling we consider intimate mixtures, putative molecular mixtures, and spatial mixtures. Intimate mixture is a term describing the situation where individual grains (μm to

mm in diameter) are mixed together. Planetary soils and regoliths are examples of such mixtures. In our usage a molecular mixture represents a case where a contaminant is trapped within a host material. To estimate the optical constants for such a mixture we linearly combine the optical constants of the candidate materials based upon their relative abundances. Because of the relatively high temperatures (>60 K, Grundy *et al.* 1999) of the uranian satellites we do not expect methane to be stable at the surface. However, because of the weak feature near 2.3 μm , we consider a molecular mixture of water ice and methane ice. In this model we envision the methane being trapped locally within the water ice. Spatial mixtures represent a linear mixing of the individual albedos of candidate materials. Such mixing is represented by relatively large scale physical features such as rocks or outcrops having spatial dimensions on the order of decimeters to meters or even kilometers. The mixing can be expressed as $R_T = R_{C1}A_{C1} + R_{C2}A_{C2} + \dots R_{Cn}A_{Cn}$, where R_T is the total reflectance and R_{Ci} and A_{Ci} are the reflectance and spatial extent of component i and it is required that $\sum A_{Ci} = 1$.

3.2.1. Optical Constants

The ice optical constants used in our spectral models come from a variety of sources, which are shown in Table III. To illustrate where each potential candidate might contribute to the Miranda spectrum we calculated the albedo for the select pure ice used in our spatial mixtures, using grain sizes representative of the best fitting mixtures discussed below. The results are shown in Fig. 3a.

Amorphous carbon provides a material that has a low albedo and is neutral in color. It also represents the end-member by-product of the processing of original hydrocarbon-bearing materials. Optical constants of amorphous carbon are from Rouleau and Martin (1991). Carbonaceous chondritic meteorites represent relatively pristine materials that could have been originally

TABLE III
Ice Optical Constants

Ice	Reference	Comments
H ₂ O, 70, 80 K (crystalline)	Grundy and Schmitt (1998) Warren (1984)	For the shortest wavelengths
NH ₃	Martonchik <i>et al.</i> (1984)	
NH ₃ · H ₂ O	R. H. Brown <i>et al.</i> (1988)	Derived, using technique of Clark and Roush (1984), extrapolated to shortest wavelength
CH ₃ OH	Cruikshank <i>et al.</i> (1998a)	Extrapolated to shortest wavelength
CH ₄	Grundy (personal communication 1999) Schmitt (personal communication 1999)	Extrapolated to shortest wavelength
CO ₂	Hansen (1997) Warren (1986)	At shorter wavelengths

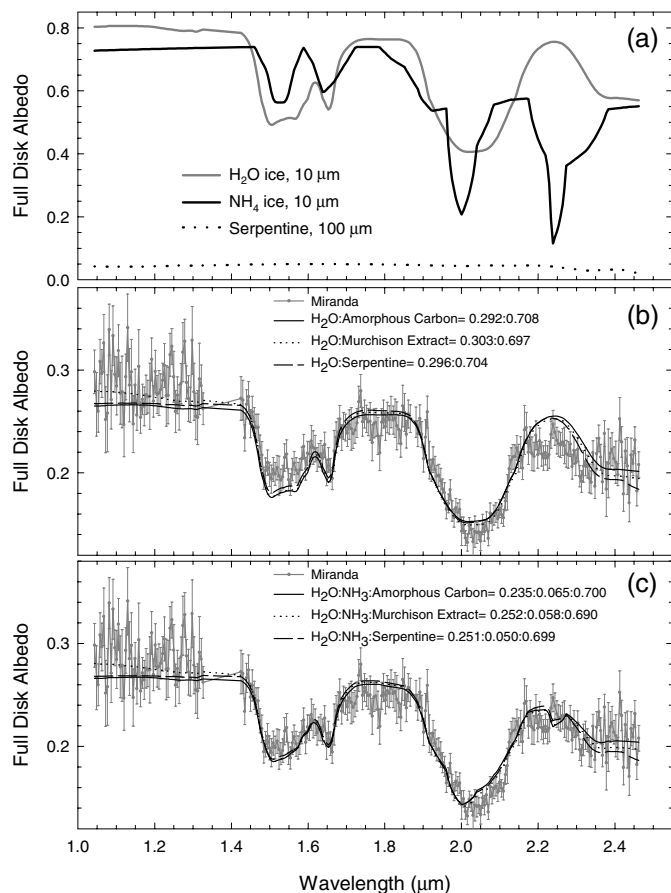


FIG. 3. (a) Calculated albedos of the individual components incorporated in the spatial mixtures. These curves help to illustrate the wavelengths where each component is contributing to the spatial mixtures. (b) Calculated two-component spatial mixtures representing the surface of Miranda (points with error bars) at near-infrared wavelengths. The curve labels indicate the relative spatial coverage of each component. (c) Calculated three-component spatial mixtures representing the surface of Miranda (points with error bars) at near-infrared wavelengths. The curve labels indicate the relative spatial coverage of each component.

incorporated into Miranda or could represent material currently being delivered to the surface of Miranda. Murchison extract, the insoluble residue from the Murchison meteorite, represents a low-albedo material with some subtle spectral features. Optical constants of Murchison extract are from Khare (personal communication, 1996). Serpentine, a hydroxylated silicate, is an aqueous weathering product of primary igneous minerals (olivine). Serpentine optical constants are derived from laboratory data presented in Roush *et al.* (1990) using the techniques described by Clark and Roush (1984). As with our pure ices, to illustrate where a select potential candidate might contribute to the Miranda spectrum we calculated the albedo for serpentine having a grain size representative of the best spatial fitting mixtures described below and the results are also shown in Fig. 3a.

Buratti *et al.* (1990) derived an average normal albedo of ~ 0.33 . Voyager imagery of Miranda revealed a heterogeneous

surface containing distinct high (~ 0.37) and low (~ 0.30) albedo regions (Buratti and Mosher 1991). Thus the spatial mixing of spectral components discussed above appears to be the most likely candidate for evaluating Miranda's near-IR spectral signature. However, the underlying cause of these albedo variations remains unknown. It is well known that grain size variations can significantly raise or lower albedos (e.g., Gaffey *et al.* 1993, and references therein). As a result, we initially model the Miranda near-IR data using intimate mixtures. In evaluating our model results we consider both models of the near-IR data and the visual geometric albedo reported for Miranda.

3.2.2. Results for Intimate Mixtures

Pure materials. We included two grain sizes in these models. Only the results for icy materials containing H_2O in some form provide a reasonable fit to the Miranda data in the region $1.45\text{--}2.5\ \mu\text{m}$. Unfortunately, in the region $1.0\text{--}1.35\ \mu\text{m}$ these pure ice mixtures typically have albedos that do not reproduce the observational data, they cannot reproduce the $2.2\text{-}\mu\text{m}$ minimum seen in the observational data, and near $0.55\ \mu\text{m}$ they have albedos (~ 0.7) that are inconsistent with those previously reported. The pure nonices are a poor fit to the Miranda data, chiefly due to the absence of water-ice features. We conclude that none of the pure mixtures provide an adequate model for the albedo of Miranda.

Two-component mixtures. We considered the situation where two distinct chemical materials are present on Miranda. Generally, models including only mixtures of icy compounds suffer the identical problems discussed for the pure materials above, poor fit in some wavelength regions and disagreement with the visual albedo values. One exception is the water-ice-ammonia mixture that is dominated by ammonia ice (98%) having a grain size of $\sim 3.3\ \text{mm}$. We do not consider this a viable result for two reasons. First, we believe the large particle diameter is being produced by the fitting routine attempting to match the overall albedo level, a difficult task for materials as transparent as ices. Second, the ammonia optical constants in the region $1.0\text{--}1.35\ \mu\text{m}$ are somewhat suspect (B. Schmitt, personal communication 2001) and may be one order of magnitude smaller than previously reported, thus requiring even larger grain sizes.

Those models that included icy and low-albedo nonicy components provide a better comparison to the visual albedo (~ 0.33). However, these also suffer from a poor fit in the 1.0- , 1.35- , and $2.2\text{-}\mu\text{m}$ regions. The additional spectral feature near $2.2\ \mu\text{m}$ seen for ammonium hydrate led us to use it as a replacement for water ice. However, the model results were not significantly improved.

Three-component mixtures. The additional weak feature near $2.2\ \mu\text{m}$ in ammonia and ammonia hydrate ice spectra may provide an improvement if these ices, water ices, and low-albedo nonicy materials are combined. However, most of the models converged to solutions where the grain diameter of one

component approached or exceeded a value where the underlying assumption of geometric optics inherent in Hapke theory was violated (Hapke 1993). The few models that converged to acceptable parameter values did not provide a significant improvement over the binary mixtures discussed above.

3.3. Spatial Mixtures

The automated spectral fitting routine described above is not fully implemented for spatial mixtures. Specifically, the grain diameters are not incorporated into the algorithm. Thus we calculate the albedo of the candidate materials and use the program to automatically derive only the relative spatial extent of each component that best reproduces the observational data. To evaluate the sensitivity of the spatial mixing to grain diameter variations we used three separate grain diameters (10, 50, and 100 μm) for most components in the spatial mixtures. However, we found that the albedo of amorphous carbon was equivalent for these three grain diameters and so we only used the albedos for the 10- μm grains in our model. In addition, we found that for Murchison extract the 50- and 100- μm grain diameter albedos were essentially equivalent and only used the albedos for the 10- and 100- μm grain diameters in our models. To illustrate where each potential ice candidate may contribute to the Miranda spectrum, we calculated albedos using grain sizes representative of the best-fitting mixtures and graphed them in Fig. 3a, along with that of the nonice material serpentine for comparison.

Two-component mixtures. Table IV shows the parameters for the best fit models of Miranda's albedo containing two and three spatial components. The models having the best χ^2 values are shown in Fig. 3b. Like the intimate mixtures discussed above, most of these mixtures have difficulty in reproducing the albedo in the region 1.04–1.36 μm . However, the albedos at 0.55 μm are more consistent with those previously reported. In all of these best results the mass fraction of water ice relative to nonice material is approximately 0.3/0.7 but there still remains a minimum near 2.2 μm in the observational data that is unexplained by any model.

Three-component mixtures. The additional weak feature near 2.2 μm in both ammonia and ammonia hydrate ice spectra may provide an improvement if these ices are included in the water-ice–nonice binary mixtures discussed in the previous section. This led us to attempt some three-component spatial models. The results for the best-fitting models of such mixtures containing ammonia ice are shown in Fig. 3c. The associated parameters are given in Table IV. Once again the abundance of ices relative to nonices is $\sim 0.3/0.7$ and the visual albedos are somewhat consistent with those previously reported. However, the ammonia ice begins to distort the short-wavelength region of the 2- μm band and we believe the sharp band near 2.25 μm is at too long a wavelength to be consistent with the Miranda data.

Using the best spatial model for the water-ice, ammonia-ice, and serpentine mixtures above we replaced the ammonia ice with ammonia hydrate ice and the resulting best fit spectra are shown

TABLE IV
Spatial Mixture Model Fits

Optical constants	Relative spatial fraction	Grain sizes ^a	χ^2 ^b	$P_{v,disk}$ ^c
Two-component mixtures				
80 K H ₂ O Amorphous carbon	0.292/0.708	0.01/0.01	5.43×10^2	0.26
80 K H ₂ O Murchison extract	0.303/0.697	0.01/0.01	4.73×10^2	0.26
80 K H ₂ O Serpentine	0.296/0.704	0.01/0.10	5.96×10^2	0.26
Three-component mixtures				
80 K H ₂ O, NH ₃ , Amorphous carbon	0.235/0.065/0.700	0.01/0.01/0.01	2.00×10^2	0.26
80 K H ₂ O, NH ₃ , Murchison extract	0.252/0.058/0.690	0.01/0.01/0.01	1.76×10^2	0.26
80 K H ₂ O, NH ₃ , Serpentine	0.251/0.050/0.699	0.01/0.01/0.10	2.01×10^2	0.27
80 K H ₂ O, 1% NH ₃ · H ₂ O, Serpentine	0.158/0.145/0.697	0.01/0.01/0.10	2.04×10^2	0.28
80 K H ₂ O, 3% NH ₃ · H ₂ O, Serpentine	0.12/0.18/0.70	0.01/0.01/0.10	2.16×10^2	0.27

^a Grain sizes (mm).

^b Reduced.

^c Albedo at 0.55 μm .

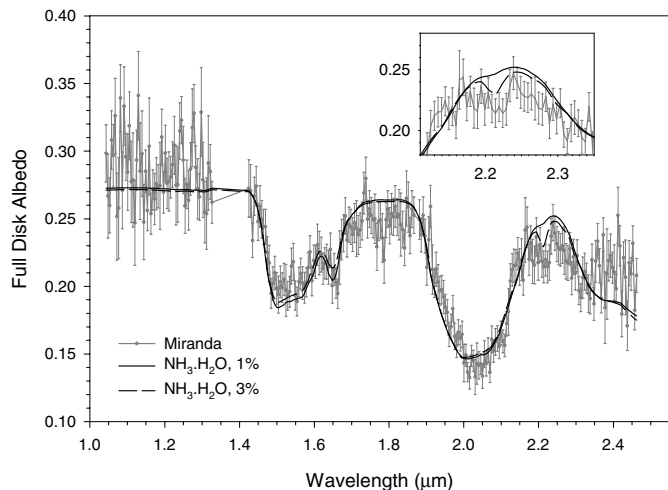


FIG. 4. Comparison of the best fitting spatial model incorporating ammonia hydrate ice (solid line) to the Miranda observations. The slight shoulder seen near $2.22 \mu\text{m}$ is stronger in higher concentrations of ammonia hydrate ices as is discussed in the text.

in Fig. 4 with the resulting parameters provided at the bottom of Table IV. While the χ^2 values are not as low as those for some of the mixtures incorporating ammonia, the resulting spectra exhibit some interesting characteristics, especially near $2.2 \mu\text{m}$. As a reminder, we derived the optical constants for the ammonia hydrate from the 1 and 3% mixture shown by R. H. Brown *et al.* (1988). R. H. Brown *et al.* (1988) also show data for 10 and 30% mixtures. Spectra of the 10 and 30% mixtures contain additional features near 1.04 and $1.25 \mu\text{m}$ that are inconsistent with the Miranda data. However, the 3 and 1% mixtures are very similar, except that the $2.2\text{-}\mu\text{m}$ feature is more readily noticeable in the 3% mixture, and it provides an apparently better fit to features in the $2.2\text{-}\mu\text{m}$ wavelength region (Fig. 4). An even better fit to the observational data might be possible with a concentration of ammonia hydrate between 3 and 10%, but the data for the optical constants at such concentrations are not available. In general, there are still very few laboratory absorption coefficients reported of ammonia hydrates. Among these there are also some discrepancies, likely owing to different compositional, physical, or measurement conditions (B. Schmitt, private communication, 2001). For example, in our values derived here there is a single broad band near $2.20\text{--}2.22 \mu\text{m}$ while in Schmitt *et al.* (1998) a broad double band is shown at $2.20\text{--}2.22 \mu\text{m}$, which may better match the spectrum of Miranda.

4. DISCUSSION

4.1. Surface Variations

Figures 2a and 2b show the albedo measurements reported in the literature and reported here, taken at NIR wavelengths. The most recent visible wavelength values taken by Karkoshka (1997) are also shown. Buratti *et al.* (1992) reported drops in

brightness levels on the order of 9% at optical wavelengths between phase angles near 1° and 2.4° . Though the data did not include Miranda, Miranda showed phase curve behavior similar to that of Ariel, Titania, and Oberon at smaller phase angles (Buratti *et al.* 1992, and Karkoshka 2001). There is a correlation with brightening and phase in the NIR Miranda data shown here, a 12 to 15% drop in brightness ($\Delta p \sim 0.04$) for a change in phase angle from 1.0° to 2.5° (Fig. 2a), which roughly agrees with the brightening trend observed by Buratti *et al.* (1992) attributable to opposition effect brightening. However, some component may also be attributable to surface albedo variations, as is likely the case in the albedo values shown in Fig. 2b, derived from observations of Miranda taken at phase angles ranging from 2.4° to 2.9° . Figure 5 shows the subobserver points on each of the dates of observation. Surely the entire hemisphere of Miranda, including some portions of the coronae, contributed to the IRTF albedo values. However, the most dominant features contributing to the signal would be the subobserver points, especially considering the phase angle curves discussed earlier from Buratti *et al.* (1990 and 1992), which show drops in brightness greater than 50% at phase angles greater than 20° . The QUIRC albedos, taken on May 22, 2000, are comparable to those derived from the UKIRT spectral data taken in June of 1999. The IRTF values, taken on May 18, 2000, however, are greater by a few percent. These differences are not greater than three standard

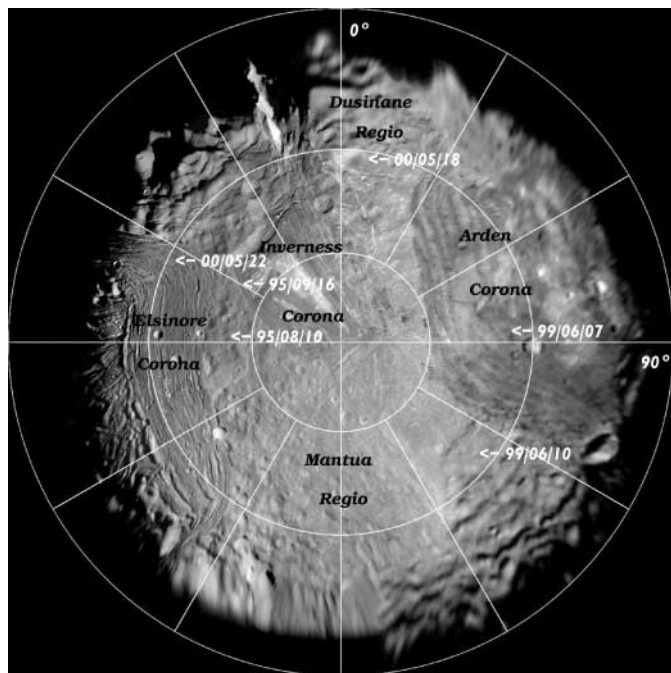


FIG. 5. The subobserver points of Miranda at the times of the data reported here and for the Baines *et al.* (1998) data. The points are indicated by date (yy/mm/dd), i.e., the Baines data by 95/08/10 and 95/09/16, the UKIRT by 99/06/07 and 99/06/10, the IRTF by 00/05/18, and the UH QUIRC data by 00/05/22. Note the subobserver points of our spectral data (99/06/07 and 99/06/10) are proximal to the Arden Corona.

deviations from the errors reported here. However, it is worth noting that the differences in the surface viewed at each observation may correspond to the albedo variations. The coronae are darker regions, by 6% (Greenberg *et al.* 1991), in the optical, and this trend may persist in the NIR as well. The Arden Corona, near the subobserver points of the UKIRT data, shows the most compelling evidence of volcanic surface flows (Croft and Soderblom 1991). The QUIRC data were taken when the subobserver points were close to coronae (Inverness and Elsinore; see Fig. 5). The IRTF data, on the other hand, were taken when a portion of the brighter Dunsinane region was facing the Earth.

4.2. Comparison with Other Outer Solar System Surfaces

The 1.65- μm water-ice feature abounds in the outer Solar System. Grundy *et al.* (1999) show that the other major uranian satellite surfaces have this feature, indicative of crystalline water ice, and they have used it in the cases of Ariel and Titania to better constrain the surface ice temperature. From these results, and their surface thermal models, they also conclude that there is at least some segregation of darker material from the brighter water ice. One may speculate that the variations in the photometry shown above may be the result of similar segregation on Miranda. Except for Titania, neither their spectral data of the other uranian satellites nor our data were very well fit by water-ice models alone, but only our Miranda spectra show evidence of any NH_3 or $\text{NH}_3 \cdot \text{H}_2\text{O}$ species specifically. No spectral observations of the uranian satellites have yielded identification of specific silicate or darkening material, or other specific volatile species on the satellite surfaces.

The crystalline ice water feature has been found in other satellites at heliocentric distances greater than Uranus, notably Triton (Cruikshank *et al.* 2000) and Charon (M. E. Brown and Calvin 2000, and Dumas *et al.* 2001). Triton, $B-V \sim 0.75$ (Buratti *et al.* 1994), and Charon, $B-V \sim 0.70$ (Tholen and Buie 1997), are somewhat redder than Miranda, $B-V \sim 0.64$ (Karkoschka 2001), and both satellites also have surface temperatures significantly lower (~ 40 K) than that of Miranda (~ 80 K). Triton's spectra show features attributable to the volatile species CO , CO_2 , CH_4 , and N_2 , as well as water ice in what may be a mixture of both crystalline and amorphous forms (Cruikshank *et al.* 2000). However, no evidence of the presence of $\text{NH}_3 \cdot \text{H}_2\text{O}$ or any NH_3 species has been found in Triton's spectra. Charon's spectrum, on the other hand, does show both the crystalline water-ice feature and the $\text{NH}_3 \cdot \text{H}_2\text{O}$ (M. E. Brown and Calvin 2000, and Dumas *et al.* 2001) feature we find in Miranda's spectrum. The 2.0- μm water band depth of Charon's spectrum also better matches that of Miranda than Triton's shallow water bands. While Triton's surface features are dissimilar to Miranda's coronae and extensional rifts, Charon's surface remains unimaged, with rotational lightcurve variations on the order of 0.1 magnitudes in the B optical filter band (Olkin *et al.* 1993, and Cruikshank *et al.* 1997). Surface maps of Charon constructed

from observational data of mutual occultations with Pluto (Buie *et al.* 1992, and Buie *et al.* 1997) do not rule out the possible presence of Miranda-like coronae and rifts on Charon. However, though Charon may have experienced accelerational and tidal heating through its interaction with Pluto in the past, neither Triton nor Charon is believed to have undergone strong heating episodes caused by passages through orbital resonances with other satellites as Miranda may have (Tittemore and Wisdom 1990). For the case of Charon, M. E. Brown and Calvin (2000) propose the crystalline ice was formed by resurfacing from micrometeorite impacts, at a rate that exceeds the transition of surface crystalline ice to amorphous phase by solar irradiation (Jenniskens *et al.* 1998).

A relatively high abundance of surface water ice has been inferred from the uniquely blue albedo of Miranda (e.g., Trilling and Brown 2000) as compared to the other uranian satellites. Observations of the Centaurs (and Kuiper belt objects) show that there is a significant color and spectral diversity ranging from slightly blue-neutral to extremely red at optical wavelengths. The spectrum of EKO 1993 SC showed the presence of absorption features consistent with light hydrocarbons, but no water ice (R. H. Brown *et al.* 1997), and the spectrum of 1996 TL₆₆ was neutral with no features (Luu and Jewitt 1998). In contrast, the spectrum of 1996 TO₆₆ showed strong near-IR absorptions characteristic of water ice (R. H. Brown *et al.* 1999a). The depth of the bands varied with rotation, suggesting a patchy ice surface distribution. The continuum of 1996 TO₆₆ was slightly blue. Most Centaurs exhibit the 2.0- μm water-ice absorption band as well. The relative strength of the absorption, however, in the Miranda spectrum, resulting in a drop in reflectance on the order of a third within the band's center, is markedly different from that of the central water band depths of a few percent observed in Centaur spectra (e.g., R. H. Brown *et al.* 1998, Kern *et al.* 2000). This may be an indication of a higher fraction of surface ice on Miranda. Some silicates in concentrations on the order of several percent by weight in intimate mixtures with water ice may deepen the relative absorption bands caused by the ice in the NIR (Clark *et al.* 1986). On the other hand, intimate mixtures with large concentrations of absorbers such as amorphous carbon, which darkens uniformly across most NIR and visible wavelengths, completely dampen the water-ice absorption band depths (Clark *et al.* 1986). The latter may be the case for the Centaurs, which have been found to have albedos at visible wavelengths of less than 8% (Parker *et al.* 1997). However, quantitative comparison is impossible because the water abundances are not provided by R. H. Brown *et al.* (1998) or Kern *et al.* (2000). The Centaur Asbolus also shows variation of water-band depth in the spectra taken by Kern *et al.* (2000). To date the crystalline ice feature at 1.65 μm has not been detected in the observed Centaur and TNO spectra (e.g., Chiron, Foster *et al.* 1999 and Luu *et al.* 2000, Pholus, and Chariklo). The amorphous ice phase transition, for impure water ice, occurs rapidly at temperatures near 142 K, and more gradually above temperatures of 100 K (Cruikshank *et al.* 1998a and Jenniskens

et al. 1998). It may be, then, that the Centaur surfaces have not undergone heating events similar to Miranda. This is not surprising if Miranda's heating is indeed attributable to passage through orbital commensurabilities (Titemore and Wisdom 1990). However, the observed Centaur spectra, with SN values ≤ 20 (e.g., Cruikshank *et al.* 1998a), may not be of sufficient sensitivity to detect the crystalline ice 1.65- μm absorption. Still, if its absence in the spectra of Centaurs is confirmed, it may affirm the pristine condition of their surfaces and constrain the amount of collisional heating. Neglecting water-ice absorption bands, Miranda's spectrum across the interval from 1.1 to 2.4 μm is notably blue, also in contrast to TNO and Centaur spectra, and the spectra of C- and D-type asteroids. As demonstrated in the modeling, this may be the result of compositional or grain size differences, which may reflect different formation or evolutionary histories of the bodies, respectively.

5. CONCLUSIONS

We have obtained a spectrum of Miranda between 1.0 and 2.5 μm which shows the 1.5- and 2.0- μm water-ice absorption features. A weak feature at 1.65 μm has been identified as being due to crystalline water ice, which may indicate heating events following condensation in excess of 100 K. Spectral reflectance models, constrained by Hapke theory to grain sizes larger than a micrometer, suggest the presence of carbonaceous or silicate contaminants at the 70% level to lower the albedo. Our best fit models include the presence of NH_3 or derivative species, specifically ammonia hydrate ($\text{NH}_3 \cdot \text{H}_2\text{O}$) at a 3% mass fraction, but this is not a unique solution. If true, except for Charon (M. E. Brown and Calvin 2000, and Dumas *et al.* 2001), this would be the only spectroscopic evidence to date of an ammonia species in the outer Solar System beyond Saturn. The suggested presence of NH_3 -water fluids may sufficiently lower melting-point temperatures and increase the degree of thermal expansion to allow for the creation of tectonic features on Miranda's surface. A significant compositional component of NH_3 would also favor previously proposed spin-out disk models for the satellite's formation (Pollack *et al.* 1991), which suggests that CH_4 and NH_3 should be the dominant C and N bearing species. Methane may have quickly evaporated from the surface, while ammonia would likely still be present (e.g., M. E. Brown 2000). The observed Centaur spectra are considerably different from Miranda's. The strength of the 2.0- and 1.5- μm bands is visibly greater in the Miranda spectrum. Miranda's blue color gradient at NIR wavelengths may be the result of grain size or compositional differences from the Centaur, TNO, and C- and D-type populations, such as a greater fraction of surface covered by water ice (e.g., Trilling and Brown 2000). Grundy *et al.* (1999) use the 1.65- μm crystalline water-ice feature to demonstrate that there may be a significant degree of segregation of water ice on Ariel and Titania, and the variations in the J, H, and K band photometry shown here may be indicative of similar segregation on Miranda's surface. The crystalline ice feature at 1.65 μm in

Miranda's spectrum has not been detected in the Centaur spectra. If proven absent, it would be evidence of clear differences in their evolutionary histories.

ACKNOWLEDGMENTS

The authors of this paper thank the staff of UKIRT, especially Thor Wold, whose assistance at the telescope was indispensable, as well as the reviewers of the manuscript for their helpful comments. J.M.B. also thanks A. Tokunaga for his help and advice with the data reduction, M. Cushing for his assistance with the IRTF imaging, and D. Tokamura for her logistical assistance. Data from JPL's Horizons ephemeris service (<http://ssd.jpl.nasa.gov/horizons.html>) and M. Showalter's Uranus Viewer plotting routine (<http://ringside.arc.nasa.gov/www/tools/tools.html>) were used for the planning and data analysis. The image of Miranda's surface for Fig. 5 was acquired from JPL's Solar System Web site and was produced by A. T. Oner. Modified IRAF scripts of B. Cavanah (1997) were used in the flux calibration of the spectral data. TLR acknowledges support from Planetary Geology and Geophysics Program via RTOP 344-30-30-01. T.R.G.'s research was supported by the Gemini Observatory, which is operated by the Association of Universities for Research in Astronomy, Inc., under a cooperative agreement with the NSF on behalf of the Gemini partnership: the National Science Foundation (United States), the Particle Physics and Astronomy Research Council (United Kingdom), the National Research Council (Canada), the Australian Research Council (Australia), CNPq (Brazil), and CONICET (Argentina). J.M.B. acknowledges support for this work from the planetary astronomy program NAG5-4495.

REFERENCES

- Allen, C. W. 1973. *Astrophysical Quantities*, Athlone Press, London.
- Baines, K. H., P. A. Yammandra-Fischer, L. A. Lebofsky, T. W. Momary, W. Golisch, C. Kaminsky, and W. Wild 1998. Near-infrared absolute photometric imaging of the uranian system. *Icarus* **132**, 266–284.
- Brown, M. E. 2000. Near-infrared spectroscopy of Centaurs and irregular satellites. *Icarus* **132**, 266–284.
- Brown, M. E., and W. M. Calvin 2000. Evidence for crystalline water and ammonia ices on Pluto's satellite Charon. *Science* **287**, 107–109.
- Brown, M. E., and C. D. Koresko 1998. Detection of water ice on the Centaur 1997 CU₂₆. *Astrophys. J.* **505**, L65–L67.
- Brown, M. E., C. D. Koresko, and G. A. Blake 1998. Detection of water ice on Nereid. *Astrophys. J.* **508**, L175–L176.
- Brown, R. H., and R. N. Clark 1984. Surface of Miranda—Identification of water ice. *Icarus* **58**, 288–292.
- Brown, R. H., D. P. Cruikshank, A. T. Tokunaga, R. G. Smith, and R. N. Clark 1988. Search for volatiles on icy satellites. I. Europa. *Icarus* **74**, 262–271.
- Brown, R. H., D. P. Cruikshank, Y. Pendleton, and G. J. Veeder 1997. Surface composition of Kuiper belt object 1993 SC. *Science* **276**, 937–939.
- Brown, R. H., D. P. Cruikshank, Y. Pendleton, and G. J. Veeder 1998. Identification of water ice on the Centaur 1997 CU₂₆. *Science* **280**, 1430–1433.
- Brown, R. H., D. P. Cruikshank, and Y. Pendleton 1999a. Water ice on Kuiper belt object 1996 TO₆₆. *Astrophys. J.* **519**, L101–L104.
- Brown, R. H., D. P. Cruikshank, Y. Pendleton, and G. J. Veeder 1999b. Water ice on Nereid. *Icarus* **139**, 374–378.
- Brown, W. M., and J. X. Luu 1997. CCD Photometry of the Centaur 1995 GO. *Icarus* **135**, 415–430.
- Buie, B., D. J. Tholen, and K. Horne 1992. Albedo maps of Pluto and Charon—Initial mutual event results. *Icarus* **97**, 211–227.
- Buie, B., E. F. Young, and R. Binzel 1997. Surface appearance of Pluto and Charon. In *Pluto and Charon* (S. A. Stern and D. J. Tholen, Eds.), pp. 269–293. Univ. of Arizona Press, Tucson.

- Buratti, B. J., and J. A. Moshier 1991. Comparative global albedo and color maps of the uranian satellites. *Icarus* **90**, 1–13.
- Buratti, B., F. Wong, and J. Moshier 1990. Surface properties and photometry of the uranian satellites. *Icarus* **84**, 203–214.
- Buratti, B. J., J. Gibson, and J. A. Moshier 1992. CCD photometry of the uranian satellites. *Astron. J.* **104**, 1618–1622.
- Buratti, B., J. D. Goguen, J. Gibson, and J. Moshier 1994. Historical photometric evidence for volatile migration on Triton. *Icarus* **101**, 303–314.
- Cavanagh, B. E. 1997. *A User's Guide to Reducing CGS4 Data with IRAF*; available at <http://www.jach.hawaii.edu/JACpublic/UKIRT/software/cgs4/iraf/>.
- Clark, R. N., and T. L. Roush 1984. Reflectance spectroscopy: Quantitative analysis techniques for remote sensing applications. *J. Geophys. Res.* **89**, 6329–6340.
- Clark, R. N., F. P. Fanale, and M. J. Gaffey 1986. Surface composition of natural satellites. In *Satellites* (J. A. Burns and M. S. Matthews, Eds.), pp. 437–491. Univ. of Arizona Press, Tucson.
- Colina, L., R. C. Bohlin, and F. Castelli 1996. The 0.12–2.5 micron absolute flux distribution of the Sun for comparison with solar analog stars. *Astron. J.* **112**, 307–315.
- Croft, S. K., and L. A. Soderblom 1991. Geology of the uranian satellites. In *Uranus* (J. T. Bergstrahl, E. D. Miner, and M. S. Matthews, Eds.), pp. 561–628. Univ. Arizona Press, Tucson.
- Cruikshank, D. P., T. L. Roush, J. M. Moore, M. V. Sykes, T. C. Owen, M. J. Bartholomew, R. H. Brown, and K. A. Tryka 1997. The surfaces of Pluto and Charon. In *Pluto and Charon* (S. A. Stern and D. J. Tholen, Eds.), pp. 221–267. Univ. Arizona Press, Tucson.
- Cruikshank, D. P., T. L. Roush, M. J. Bartholomew, T. R. Geballe, Y. J. Pendleton, S. M. White, J. F. Bell, J. K. Davies, T. C. Owen, C. De Bergh, D. J. Tholen, M. P. Bernstein, R. H. Brown, K. A. Tryka, and C. M. Dalle Ore 1998a. The composition of Centaur 5145 Pholus. *Icarus* **135**, 389–407.
- Cruikshank, D. P., T. L. Roush, T. C. Owen, E. Quirico, and C. DeBergh 1998b. The surface composition of Triton, Pluto, and Charon. In *Solar System Ices* (B. Schmitt, C. de Bergh, and M. Festou, Eds.), pp. 655–684. Kluwer Academic, Dordrecht.
- Cruikshank, D. P., B. Schmitt, T. L. Roush, T. C. Owen, T. R. Geballe, C. De Bergh, M. J. Bartholomew, C. M. Dalle Ore, S. Douste, and R. Meier 2000. Water ice on Triton. *Icarus* **147**, 309–316.
- Davies, J. K., N. McBride, S. L. Ellison, S. F. Green, and D. R. Ballantyne 1998. Visible and infrared photometry of six centaurs. *Icarus* **134**, 213–227.
- Dumas, C., R. J. Terrile, R. H. Brown, G. Schneider, and B. A. Smith 2001. Hubble Space Telescope NICMOS spectroscopy of Charon's leading and trailing hemispheres. *Astron. J.* **121**, 1163–1170.
- Foster, M. J., S. F. Green, N. McBride, and J. K. Davies 1999. Detection of water ice on 2060 Chiron. *Icarus* **141**, 408–410.
- Gaffey, S. J., L. A. McFadden, D. Nash, and C. M. Pieters 1993. Ultraviolet, visible, and near-infrared reflectance spectroscopy: Laboratory spectra of geologic materials. In *Remote Geochemical Analysis: Elemental and Mineralogical Composition* (C. M. Pieters and P. A. J. Englert, Eds.), pp. 43–77. Cambridge Univ. Press, New York.
- Greenberg, R., S. K. Croft, D. M. Janes, J. S. Kargel, L. A. Lebofsky, J. I. Lunine, R. L. Marcialis, H. J. Melosh, G. W. Ojakangas, and R. G. Strom 1991. Miranda. In *Uranus* (J. T. Bergstrahl, E. D. Miner, and M. S. Matthews, Eds.), pp. 693–735. Univ. of Arizona Press, Tucson.
- Grundy, W. M., and B. Schmitt 1998. The temperature-dependent near-infrared absorption spectrum of hexagonal H₂O ice. *J. Geophys. Res.* **103**, 25,809–25,822.
- Grundy, W. M., M. W. Buie, J. A. Stansberry, J. R. Spencer, and B. Schmitt 1999. Near-infrared spectra of icy outer Solar System surfaces: Remote determination of H₂O ice temperatures. *Icarus* **142**, 536–549.
- Hansen, G. B. 1997. The infrared absorption spectrum of carbon dioxide ice from 1.3 to 333 μm . *J. Geophys. Res.* **102**, 21,569–21,587.
- Hapke, B. 1993. *Reflectance and Emissance Spectroscopy*. Cambridge Univ. Press, New York.
- Helfenstein, P., J. Veverka, and P. C. Thomas 1988. Uranus satellites—Hapke parameters from Voyager disk-integrated photometry. *Icarus* **74**, 231–239.
- Jacobson, R. A., J. K. Campbell, A. H. Taylor, and S. P. Synnott 1992. The masses of Uranus and its major satellites from Voyager tracking data and earth-based uranian satellite data. *Astron. J.* **103**, 2068–2078.
- Jenniskens, P., D. F. Blake, and A. Kouchi 1998. Amorphous water ice. In *Solar System Ices* (B. Schmitt, C. de Bergh, and M. Festou, Eds.), pp. 139–155. Kluwer Academic, Dordrecht.
- Karkoschka, E. 1997. Rings and satellites of Uranus: Colorful and not so dark. *Icarus* **125**, 348–363.
- Karkoschka, E. 2001. Comprehensive photometry of the rings and 16 satellites of Uranus with the Hubble Space Telescope. *Icarus* **151**, 51–68.
- Kern, S. D., D. W. McCarthy, M. W. Buie, R. H. Brown, H. Campins, and M. Rieke 2000. Compositional variation on the surface of Centaur 8405 Asbolus. *Astrophys. J.* **542**, L155–L159.
- Kesten, P. R., J. K. Davies, D. P. Cruikshank, and T. L. Roush 1998. Uranian satellites and Triton: JHK photometry. *Bull. Am. Astron. Soc.* **30**, 1099.
- Kuiper, G. P. 1949. The fifth satellite of Uranus. *Publ. Astron. Soc. Pacific* **61**, 129.
- Luu, J. X., and D. C. Jewitt 1998. Optical and infrared reflectance spectrum of Kuiper belt object 1996 TL66. *Astrophys. J.* **494**, L117–L120.
- Luu, J. X., D. C. Jewitt, and C. A. Trujillo 2000. Water ice in 2060 Chiron and its implications for Centaurs and Kuiper belt objects. *Astrophys. J.* **531**, L151–L154.
- Marcialis, R., and R. Greenberg 1987. Warming of Miranda during chaotic rotation. *Nature* **328**, 227–229.
- Martonchik, J. V., G. S. Orton, and J. F. Appleby 1984. Optical properties of NH₃ ice from the far infrared to the near ultraviolet. *App. Opt.* **23**, 541–547.
- Olkin, C. B., L. A. Young, J. L. Elliot, D. T. Tholen, and M. W. Buie 1993. Individual light curves of Pluto and Charon. *Bull. Am. Astron. Soc.* **25**, 1132.
- Owen, T. C., D. P. Cruikshank, C. M. Dalle Ore, T. R. Geballe, T. L. Roush, and C. de Bergh 1999. Detection of water ice on Saturn's satellite Phoebe. *Icarus* **139**, 379–382.
- Parker, J. W., S. A. Stern, M. C. Festou, and M. F. A'Hearn 1997. Ultraviolet observations of Chiron with the HST/FOS: Examining a Centaur's gray matter. *Astron. J.* **113**, 1899–1908.
- Pollack, J. B., J. I. Lunine, and W. C. Tittlemore 1991. Origin of the uranian satellites. In *Uranus* (J. T. Bergstrahl, E. D. Miner, and M. S. Matthews, Eds.), pp. 469–512. Univ. of Arizona Press, Tucson.
- Press, W. H., S. A. Teukolsky, W. T. Vetterling, and B. P. Flannery 1992. *Numerical Recipes in Fortran: The Art of Scientific Computing*, 2nd ed. Cambridge Univ. Press, New York.
- Rayner, J. T., D. W. Toomey, P. M. Onaka, A. J. Denault, W. E. Stahlberger, D. Y. Watanabe, and S. Wang 1998. SpeX: A medium-resolution IR spectrograph for IRTF. *Proc. SPIE* **3354**, 468–479.
- Rouleau, F., and P. G. Martin 1991. Shape and clustering effects on the optical properties of amorphous carbon. *Astrophys. J.* **377**, 526–540.
- Roush, T. L. 1994. Charon: More than water ice?. *Icarus* **108**, 243–254.
- Roush, T. L., J. B. Pollack, F. C. Witteborn, J. D. Bregman, and J. P. Simpson 1990. Ice and minerals on Callisto: A reassessment of the reflectance spectra. *Icarus* **86**, 355–382.
- Roush, T. L., D. P. Cruikshank, J. B. Pollack, E. F. Young, and M. J. Bartholomew 1996. Near-infrared spectral geometric albedos of Charon and Pluto: Constraints on Charon's surface composition. *Icarus* **119**, 214–218.

- Schmitt, B., E. Quirico, F. Trotta, and W. M. Grundy 1998. Optical properties of ices from UV to infrared. In *Solar System Ices* (B. Schmitt, C. de Bergh, and M. Festou, Eds.), pp. 192–240. Kluwer Academic, Dordrecht.
- Tholen, D. J., and M. W. Buie 1997. Bulk properties of Pluto and Charon. In *Pluto and Charon* (S. A. Stern and D. J. Tholen, Eds.), pp. 193–219. Univ. of Arizona Press, Tucson.
- Tittemore, W. C., and J. Wisdom 1990. Tidal evolution of the uranian satellites. III. Evolution through the Miranda–Umbriel 3 : 1, Miranda–Ariel 5 : 3, and Ariel–Umbriel 2 : 1 mean-motion commensurabilities. *Icarus* **85**, 394–443.
- Trilling, D. E., and R. H. Brown 2000. Red, gray, and blue: Near infrared spectroscopy of faint moons of Uranus and Neptune. *Icarus* **148**, 301–306.
- Veverka, J., R. H. Brown, and J. F. Bell 1991. Uranus satellites: Surface properties. In *Uranus* (J. T. Bergstralh, E. D. Miner, and M. S. Matthews, Eds.), pp. 528–560. Univ. of Arizona Press Tucson.
- Warren, S. W. 1984. Optical constants of ice from the ultraviolet to the microwave. *Appl. Opt.* **23**, 1206–1225.
- Warren, S. W. 1986. Optical constants of carbon dioxide ice. *Appl. Opt.* **25**, 2650–2674.